CHINESE OPTICS LETTERS

Vol. 21, No. 12 | December 2023

Tilted spatiotemporal optical vortex with partial temporal coherence [Invited]

Jordan Adams[1,2] and Andy Chong[3*]

[1] Department of Electro-Optics and Photonics, University of Dayton, Dayton, Ohio 45434, United States

[2] Optics and Photonics, Riverside Research Institute, Beavercreek, Ohio 45431, United States

[3] Department of Physics, Pusan National University, Geumjeong-Gu, Busan 46241, Republic of Korea

*Corresponding author: chong0422@pusan.ac.kr

Received May 29, 2023 | Accepted July 27, 2023 | Posted Online December 8, 2023

We report the experimental and theoretical investigation of tilted spatiotemporal optical vortices with partial temporal coherence. The theoretical study shows that the instantaneous spatiotemporal optical vortex is widely variable with the statistical orbital angular momentum (OAM) direction. While decreasing temporal coherence results in a larger variability of OAM tilt, the average OAM direction is relatively unchanged.

Keywords: STOVs; tilted optical vortex; partial temporal coherence; optical OAM; partially coherent OAM.

DOI: 10.3788/COL202321.120002

1. Introduction

Light-carrying orbital angular momentum (OAM) has been an active research topic for decades, traditionally as vortex beams that have longitudinal OAM with spatial phase singularities. Such vortex beams have proven to be useful for a wide variety of applications, such as free-space communications, particle manipulation, quantum entanglement, imaging, and more[1,2]. Recently, transverse OAM states with spatiotemporal vortices (STOVs) have been demonstrated as having tilted spatiotemporal vortices[3,4]. Having full spatiotemporal control of the OAM states may open up new possibilities for the applications listed above.

In certain applications, partial coherence is beneficial, especially when utilizing light with OAM[5,6]. For example, partial spatial coherence improves the signal-to-noise ratio with longitudinal OAM communication and reduces speckle in imaging[5]. On top of improved performance, incoherent sources are cheaper and have a simpler setup. Partial temporal coherence sources may offer such benefits for STOVs. STOVs with partial temporal coherence have been recently investigated and demonstrated[7,8]. However, there has not been a report of tilted STOVs with partial temporal coherence.

Here, we investigate the tilted STOV with partial temporal coherence. We theoretically study the time-varying nature of the OAM direction of a partially coherent STOV. We also present experimental evidence of a partially coherent STOV with tilted OAM. Tilted vortices with partial temporal coherence may be beneficial for future applications such as communication and particle manipulation, especially with low-cost and simple-to-use optical sources.

2. Simulation

We first simulate a STOV with partial temporal coherence. To simulate partial coherence, we apply a random phase on each temporal frequency of a coherent wave packet[8,9]. The probability of the phase follows a normal random distribution where we control the amount of randomness with the standard deviation, σ_ω. On top of the partial temporal coherence, we add a spatiotemporal spiral phase to generate a STOV with a transverse OAM[8]. As the STOV passes through a pair of rotated cylindrical lenses, the OAM direction is tilted following the method in Ref. [4]. To observe a typical behavior of the tilted incoherent STOV, we use parameters near our experiment values discussed later, a Gaussian beam with 1 mm diameter and a spectrum that is also assumed to be Gaussian with 2.35 THz FWHM. Figures 1(a) and 1(b) show a typical iso-intensity profile of the simulation result.

From observation, the time-varying vortex angle clearly takes on a wide range of values. The partially coherent field itself has pulse-like fluctuations of intensity with temporal width near the coherence time[10], and we see that each fluctuation tends to have an isolated vortex in a certain direction. However, as shown in Fig. 1(c), some areas can have tilt angles that smoothly vary with time over one fully connected vortex. The random temporal phase causes fluctuations in the amount of transverse OAM and the spatial location of the singularity[8]. The combination of such time-varying transverse OAM components with the longitudinal OAM by the cylindrical lens pair results in the time-varying random vortex direction. The next step is to measure the time-varying OAM direction. However, because the STOVs are in random positions relative to the center axis, the

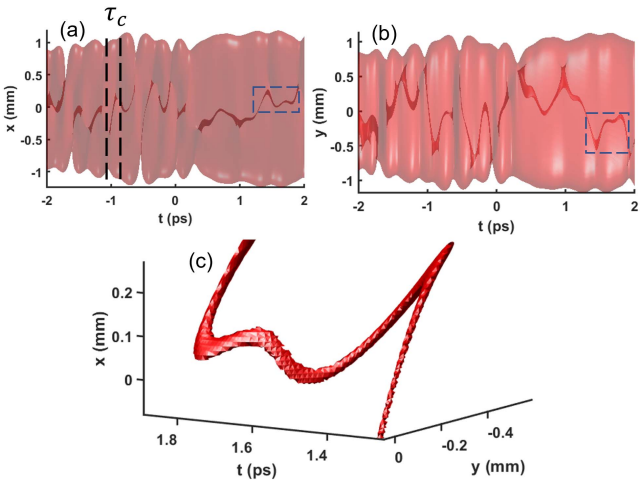

Fig. 1. Iso-intensity of simulated partially coherent tilted vortices in (a) *x*-*t* view and (b) *y*-*t* view. The coherence time, $\tau_c = 186$ fs, is overlaid in one section to highlight the typical length of the intensity fluctuations and vortices. (c) A small region of the same realization shown to highlight the random vortex tilt path.

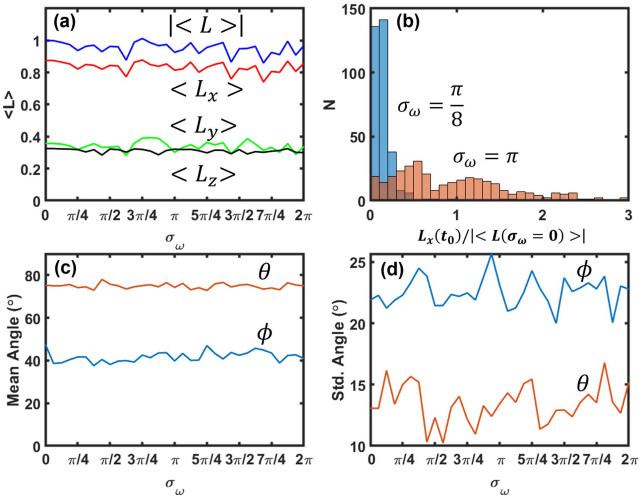

Fig. 2. (a) Magnitude of mean OAM vector and mean OAM vector components for decreasing coherence; (b) *x*-component OAM histogram for $\sigma_\omega = \frac{\pi}{8}$ and $\sigma_\omega = \pi$; (c) mean OAM angles; and (d) variance of OAM angles for decreasing coherence.

best choice of sampling location and size is not clear due to the addition of extrinsic OAM. While measuring the intrinsic OAM vector would give a reliable angle, adding extrinsic OAMs from sampling off-center could potentially give an incorrect direction measurement. Sampling at the center of each vortex would certainly be a good choice to eliminate extrinsic contributions. However, for our case, we wish to understand how a stationary observer or particle would experience the partially coherent STOV. We calculate the OAM vector within a small volume at the wave-packet center ($200\,\mu\text{m} \times 200\,\mu\text{m} \times 33$ fs) while the volume is scanned in time. The volume is temporally narrower than the coherence time (186 fs) to measure the fast-varying OAM angle, while the spatial region is small to capture only the OAM vector near the vortices crossing the center. As the spatial area is reduced in size, the values converge to what is expected and further shrinking beyond our chosen integration region, gives no change in average values. The OAM vector is[3]

$$\vec{L}(t_0) = \iiint_V \vec{r} \times \text{Imag}(\psi^* \nabla \psi) \mathrm{d}V, \tag{1}$$

where ψ is the field, and $\vec{r}$ and V are the distance vector and integration volume, both centered on the propagation axis at sampling location $t = t_0$. Furthermore, we define the normalized time-average mean OAM vector as the mean over the entire temporally scanned region, T, normalized to the vector magnitude of the fully coherent case ($\sigma_\omega = 0$),

$$\langle \vec{L} \rangle = \frac{\frac{1}{T}\int \vec{L}(t_0)\mathrm{d}t_0}{\frac{1}{T}\left|\int \vec{L}(t_0, \sigma_\omega = 0)\mathrm{d}t_0\right|}, \tag{2}$$

and the vector components are $\langle \vec{L} \rangle \cdot e_i = \langle L_i \rangle$, where $i = x, y, z$. Figure 2(a) shows the time-average OAM vector components as well as their magnitude as a function of the coherence. Although the angle of the STOV fluctuates in time, it is noteworthy that the time-average vector components do not change much by the source randomness. Figure 2(b) gives a histogram of the *x*-component for $\sigma_\omega = \frac{\pi}{8}$ and $\sigma_\omega = \pi$. As coherence is reduced, the OAM distribution broadens. However, the mean OAM components are more or less the same as shown in Fig. 2(a).

Next, we calculate the direction of the OAM from the time-varying OAM vector components using the spherical polar system aligned to the propagation axis,

$$\phi(t_0) = \arctan\left(\frac{L_y(t_0)}{L_x(t_0)}\right) \tag{3}$$

as the azimuthal angle and

$$\theta(t_0) = \arctan\left(\frac{\sqrt{(L_x(t_0))^2 + (L_y(t_0))^2}}{L_z(t_0)}\right) \tag{4}$$

as the polar angle. This can also be related to the tilt from the original STOV direction before the cylindrical lens system, which is purely transverse in the *x* direction. The tilt angle, γ from the original transverse OAM direction is given by $\gamma = \arccos(\cos(\phi)\sin(\theta))$. However, the tilt angle does not tell the OAM direction, but it only tells how much the OAM is off from the original direction. Therefore, to designate the OAM directions, we will use ϕ and θ. The time-average and standard deviation of angles are shown in Figs. 2(c) and 2(d), respectively. The mean and standard deviation of the angles remain mostly the same, regardless of the degree of coherence. The mean polar angle is between 74 deg and 77 deg, while the azimuthal angle is between 39 deg and 45 deg. Because we are sampling with a

moving time window with a limited number of time samples, even the fully coherent tilted vortex has a large variance (i.e., each time slice has a different OAM value).

However, the angles clearly become more random as the source coherence decreases. To illustrate this, we plot the magnitude and angles together as points in a polar cross-sectional plot in Fig. 3, with each point representing a time sample. The polar angle in the plot is the $\phi(t_0)$ in Eq. (3), and the radial value is $r(t_0) = \frac{|L(t_0)|\sin(\theta(t_0))}{|\langle L(\sigma_\omega=0)\rangle|}$, the sine of the polar angle multiplied by the OAM magnitude, again normalized to the fully coherent average OAM magnitude. At high coherence, the values congregate near $r = 0$ because most of the STOV is localized in time. In addition, the magnitude smoothly increases and decreases in time. As coherence drops, the OAM magnitude and direction become more dispersed, shown as spreading on the polar plot around $r = 0$ [Fig. 3(b)]. At the higher randomness of $\sigma_\omega = \pi$, the plot randomly spreads further. Therefore, though the perceived standard deviation in angles to an observer is not changed much, the angles are more random for incoherent sources. Since the time-averaged OAM magnitude and direction are stable, it is believed that the incoherent tilted OAM can be used for applications with long response times.

Finally, as we cannot directly measure time-varying OAM or OAM tilt direction, we generate a delayed reference interference pattern. The delayed reference interference patterns can be used to reveal the average tilt-angle by tracking the singularity position[8] and are represented by the equation,

$$I(x,y,\tau) = \int \left| E_o(x,y,t) + E_r\left(x,y,t+\frac{\tau}{c}\right)\right|^2 \mathrm{d}t, \qquad (5)$$

where E_o and E_r are the object and reference, τ is the delay in spatial units, and c is the speed of light. The reference is the incoherent source itself without OAM.

Each interference pattern reveals the time-average spatial phase information at a specific delay, with the singularities of the vortices identifiable by a fork interference fringe (annotated with arrows). Figures 4(a) and 4(b) show the interference patterns at a separation delay of 100 fs or 30 μm, about half the coherence length, with the fork-shaped fringes location annotated with arrows. The direction of the OAM can be revealed

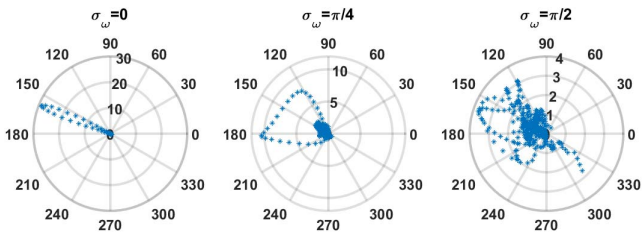

Fig. 3. $|L(t_0)|$, $\theta(t_0)$ and $\phi(t_0)$ plotted together for each time instance for different levels of randomness. OAM magnitude, polar angle, and azimuthal angle randomness increase with source randomness as shown by high-density areas broadening.

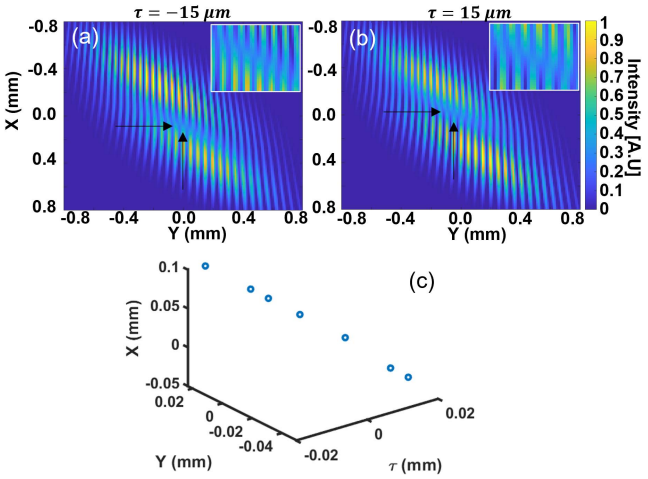

Fig. 4. (a), (b) Simulated interference pattern at two reference delays of 30 μm separation; (c) 3D trace of the singularity.

by the fork fringe movement, ΔX and ΔY, over the delay difference $\Delta\tau$. Figure 4(c) plots the fork location over delay positions separated by 5 μm, revealing the time average tilt direction of the OAM. At greater than 30 μm delay, the interference fringe visibility of the forks starts to decrease significantly. We define angles observed from the interference pattern in the spherical coordinates as earlier so that $\phi_I = \arctan(\frac{\Delta Y}{\Delta X})$ is the azimuthal angle and $\theta_I = \arctan(\frac{\sqrt{(\Delta X)^2+(\Delta Y)^2}}{\Delta\tau})$ is the polar angle of the interference pattern. With $\Delta X = 121$ μm, $\Delta Y = 65.3$ μm, and $\Delta\tau = 30$ μm, the azimuthal and polar angles are $\phi_I = 28.3$ deg and $\theta_I = 77.7$ deg. Unfortunately, since the reference also varies in time, the measured angles from the interference pattern are not exactly the time-average OAM directional angles. They only tell the average direction of the OAM roughly. As a consequence,

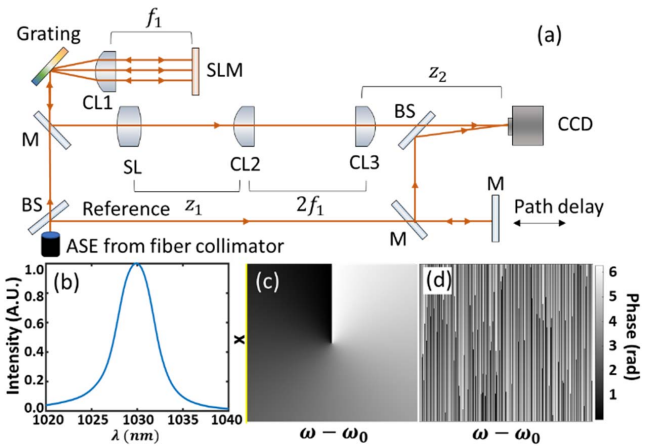

Fig. 5. (a) Experimental setup. BS, beam splitter; CL, cylindrical lenses with focal length $f_1 = 100$ mm; SLM, spatial light modulator; M, mirror; SL, spherical lens with focal length $f = 300$ mm; distances $z_1 = 200$ mm and $z_2 = 200$ mm. (b) Spectrum of ASE light source coming from Yb-fiber ring cavity; (c) phase map of the pulse shaper SLM, which applies an x–ω spatiotemporal spiral phase; (d) same phase map, including random phase expected with ASE.

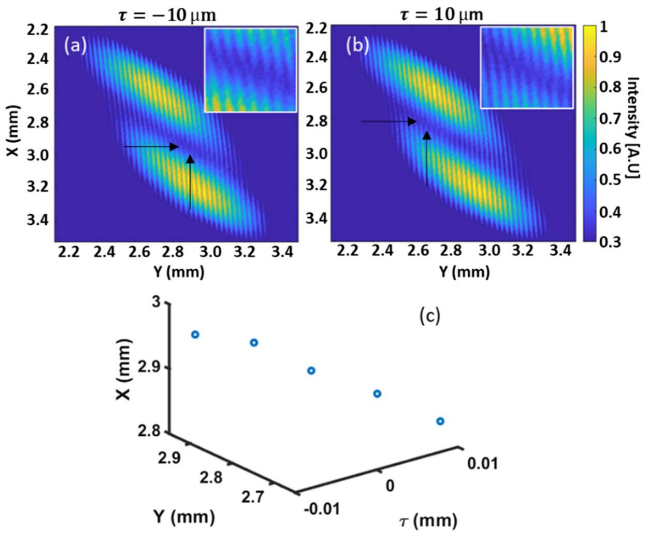

Fig. 6. (a), (b) Experimental interference patterns at two reference delays showing moving singularity indicated by arrows. The coloring minimum value is limited to 0.3 of the normalized intensity to improve the fringe contrast. Insets show enlarged areas containing the singularity interference fork. (c) Plot of vortex singularity points position versus delay.

θ_I matches well with the value directly calculated in simulation, while ϕ_I is about 10 deg off.

3. Experiment

The experimental setup is shown in Fig. 5(a) and follows the method described in Ref. [4]. The light source is amplified spontaneous emission (ASE) from an ytterbium fiber ring cavity with spectrum shown in Fig. 5(b). A pulse shaper with a spiral phase is used to add transverse OAM to the source [phase map in Fig. 5(c)]. As an example of the full spatiotemporal phase, the spiral phase combined with the expected random phase from ASE is shown in Fig. 5(d). Rotated cylindrical lenses are used to spatiotemporally tilt the vortices. The cylindrical lens pair is rotated at 45 deg, which gives the maximum tilt angle[4]. A reference, which is the original ASE with variable delay, is used to record the time-average interference onto a CCD.

Figure 6(a) and 6(b) show interference patterns at delays separated by 5 μm. Figure 6(c) plots the fork fringe location for each delay. In the experimental case, the fork fringe visibility begins degrading with distances over 20 μm. With $\Delta X = 145\,\mu\text{m}$, $\Delta Y = 195\,\mu\text{m}$, and $\Delta\tau = 20\,\mu\text{m}$, the angles are $\phi_I = 53.4$ deg and $\theta_I = 85.3$ deg. The angles are off from the simulated result, since the measurement is done with a time-varying reference beam. However, the measurement clearly shows that the OAM is tilted.

In conclusion, we have demonstrated tilted STOVs with partial temporal coherence. We first explored the time-varying OAM and direction in simulation, which were then demonstrated experimentally. We believe cheap and simple light sources such as ASE will encourage further research and applications of tilted STOVs such as communications and particle manipulation. Since the average is largely unaffected, applications utilizing only average OAM would greatly benefit.

Acknowledgement

This work was supported by the National Research Foundation of Korea (NRF), funded by the Korea government (MSIT) (No. 2022R1A2C1091890).

References

1. Y. Shen, X. Wang, Z. Xie, C. Min, X. Fu, Q. Liu, M. Gong, and X. Yuan, "Optical vortices 30 years on: OAM manipulation from topological charge to multiple singularities," Light Sci. Appl. **8**, 90 (2019).
2. D. Gao, W. Ding, M. Nieto-Vesperinas, X. Ding, M. Rahman, T. Zhang, C. Lim, and C. Qiu, "Optical manipulation from the microscale to the nanoscale: fundamentals, advances and prospects," Light Sci. Appl. **6**, e17039 (2017).
3. A. Chong, C. Wan, J. Chen, and Q. Zhan, "Generation of spatiotemporal optical vortices with controllable transverse orbital angular momentum," Nat. Photonics **14**, 350 (2020).
4. Y. Zang, A. Mirando, and A. Chong, "Spatiotemporal optical vortices with arbitrary orbital angular momentum orientation by astigmatic mode converters," Nanophotonics **11**, 745 (2022).
5. J. Zeng, R. Lin, X. Liu, C. Zhao, and Y. Cai, "Review on partially coherent vortex beams," Front. Optoelectron. **12**, 229 (2019).
6. M. Dong, C. Zhao, Y. Cai, and Y. Yang, "Partially coherent vortex beams: fundamentals and applications," Sci. China Phys. Mech. Astron. **64**, 224201 (2021).
7. M. W. Hyde, IV, O. Korotkova, and M. F. Spencer, "Partially coherent sources whose coherent modes are spatiotemporal optical vortex beams," J. Opt. **25**, 035606 (2023).
8. A. Mirando, Y. Zang, Q. Zhan, and A. Chong, "Generation of spatiotemporal optical vortices with partial temporal coherence," Opt. Express **29**, 30426 (2021).
9. Q. Li, H. Zhang, X. Shen, H. Hao, and M. Gong, "Phenomenological model for spectral broadening of incoherent light in fibers via self-phase modulation and dispersion," J. Opt. **18**, 115503 (2016).
10. J. Goodman, *Statistical Optics* (Wiley-Interscience, 2000).